ACS APPLIED MATERIALS & INTERFACES

Research Article

www.acsami.org

Soluble Transition Metal Oxide/Polymeric Acid Composites for Efficient Hole-Transport Layers in Polymer Solar Cells

Junghwan Kim,[†] Heejoo Kim,*[,‡] Geunjin Kim,[§] Hyungcheol Back,[§] and Kwanghee Lee*[,†,‡,§]

[†]Department of Nanobio Materials and Electronics, [‡]Heeger Center for Advanced Materials & Research Institute for Solar and Sustainable Energies, [§]School of Materials Science and Engineering, Gwangju Institute of Science and Technology, Gwangju 500-712, Republic of Korea

Supporting Information

ABSTRACT: We report a new method for developing a low-temperature solution processed vanadium oxide (s-VO_x) and poly(4-styrene sulfonic acid) (PSS) composite to act as an efficient hole-transport layer (HTL) in polymer solar cells (PSCs). By compositing the s-VO_x and PSS (s-VO_x:PSS), the work function values of the s-VO_x:PSS changed from 5.0 to 5.3 eV. Therefore, the energy level barrier between the HTL and organic active layer decreased, facilitating charge injection/extraction at the interfaces. In addition, the s-VO_x:PSS films were denser and had more pin-hole-free surfaces than pristine s-VO_x films, resulting in enhanced PSC performance due to significantly decreased leakage currents and excellent device stability in ambient condition. Because our approach of combining soluble transition metal oxide (TMO) and polymeric acid shows dramatically better performance than pristine TMO, we expect that it can provide useful guidelines for the synthesis and application of TMOs for organic electronics in the future.

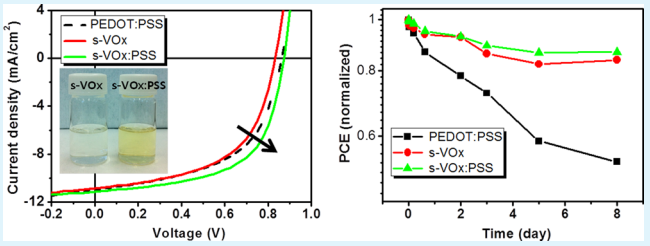

KEYWORDS: *solution-processable transition metal oxides, polymeric acids, hole-transport layers, polymer solar cells*

1. INTRODUCTION

Bulk heterojunction (BHJ) polymer solar cells (PSCs) comprising π-conjugated polymers (π-CPs) and fullerene derivatives have attracted much attention as future renewable energy sources due to their low production cost, easy manufacturing, light weight, and mechanical flexibility.[1,2] Recently, the power conversion efficiency (PCE) of PSCs has exceeded 10%, indicating an optimistic future. However, it is still challenging to improve the PCE of PSCs in commercial applications. The conventional structure of PSCs uses a metal-organic semiconductor (active layer)-metal configuration (M-O-M). Therefore, after a charge carrier has been generated in the active layer, efficient charge injection/extraction at the interfaces of the active layer and metal electrodes is critical for improving the PCE. However, there are generally significant energy losses in such M-O-M structures due to incompatibilities at the interface of the photoactive layer and electrodes, including large contact resistance, misalignment of energy levels, and increased charge recombination by surface defect sites.[3,4] Therefore, interfacial layers have been introduced between the metal electrode and the active layer to facilitate charge injection/extraction by reducing the charge recombination, increasing the internal electric field, and aligning the energy level at the interface.

During the last decade, significant efforts have been made to develop an excellent interfacial layer using transition metal oxides (TMOs) such as titanium oxide (TiO_x) and zinc oxide (ZnO) as electron transport layers (ETL), and nickel oxide (NiO), molybdenum oxide (MoO_3), and vanadium oxide (V_2O_5) as hole transport layers (HTL); these metal oxides have excellent stability, charge transport properties, and charge selectivity.[5−9] However, despite the great potential of TMOs, surface trap sites and low charge carrier density, which originated from structural imperfection of TMOs, often cause increased charge recombination and energy level misalignment at the interface of PSCs, thereby reducing the PCE of PSCs.[10−14] To alleviate these issues, two methods have been developed and shown to improve the PCE. The first method involves modification of the surface of electron transporting (ET)-TMOs (e.g., TiO_x or ZnO) by incorporating thin layers of organic conjugated/nonconjugated polyelectrolytes (CPE/NCPE)[15,16] or a C_{60}-based self-assembly monolayer (SAM).[17,18] The second method is to dope ETL-TMOs with alkali metals.[19]

A thin organic layer of CPE/NCPE or SAM on TMO layers can lower the work function (WF) of TMOs by forming a permanent dipole at the interface, hence improving electron extraction from the active layer to the cathode electrode.[15,16] Thus, this method is more efficiently applicable to ET-TMOs; it is not suitable for hole transporting TMOs (HT-TMOs) such as NiO, MoO_3, and V_2O_5. In addition, the double layer TMO/organic layer structure does not allow easy and simple fabrication, an advantage of PSCs. The other surface modification approach is to dope the HT-TMOs. Because the

Received: October 4, 2013
Accepted: December 26, 2013
Published: December 26, 2013

dopant can induce a charge transfer from the TMOs to itself and vice versa, the electronic properties of TMOs, such as WF and charge carrier density, can be easily modified within a single interfacial layer.

In this work, we developed a novel HT-TMO composed of a low-temperature solution processed vanadium oxide (s-VO_x) and poly(4-styrene sulfonic acid) (PSS) composite (s-VO_x:PSS) for highly efficient and stable PSCs. The polymeric acid, PSS, was used as a dopant to adjust the WF of the s-VO_x, which improved charge injection/extraction by reducing energy level barriers between the HTL and organic active layers. The s-VO_x:PSS showed more dense and pin-hole free surfaces compared to pristine s-VO_x films due to the polymeric structural properties of the PSS. These improved electrical and physical properties of the s-VO_x:PSS composite films significantly enhanced charge injection/extraction and reduced leakage currents in the PSCs, thereby leading to an improved PCE. In addition, the PSCs with the s-VO_x:PSS showed promising long-term stability in ambient condition without any encapsulation.

2. RESULTS AND DISCUSSION

2.1. Synthesis and Characterization of s-VO_x and s-VO_x:PSS. Figure 1a,b shows the molecular structure of

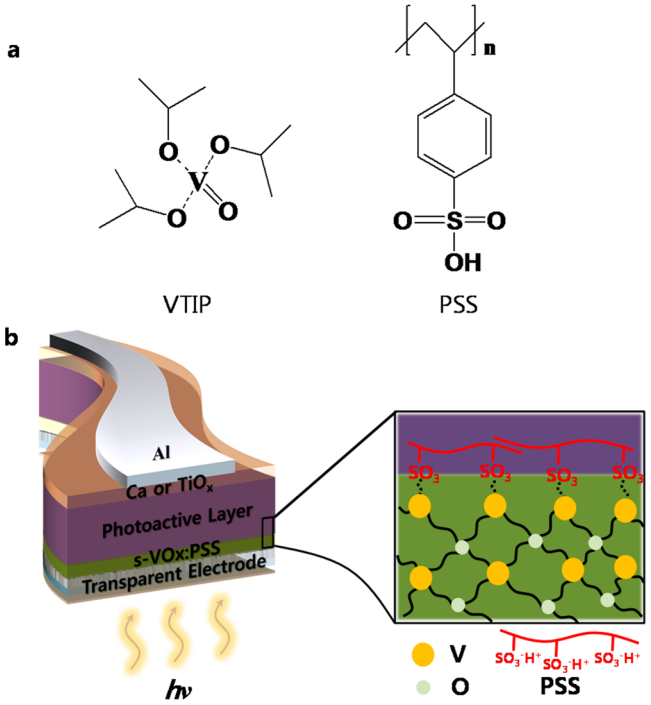

Figure 1. (a) Molecular structures of vanadium-oxytri-isopropoxide (VTIP) and PSS. (b) Device structure of PSCs incorporating s-VO_x:PSS composite as a hole transport layer.

vanadium-oxytri-isopropoxide (VTIP) and PSS and the device structure used in this study. Sol–gel derived s-VO_x was prepared using a mixed solution of the precursor, VTIP, and isopropyl alcohol (IPA) in ambient air.[20] To synthesize s-VO_x:PSS, PSS was mixed with the prepared s-VO_x solution. Because PSS has acidic and polymeric properties, it was used as an oxidation dopant and a structural template in a p-type conducting polymer, poly(3,4-ethylene dioxythiophene):(polystyrene sulfonic acid) (PEDOT:PSS).[21,22] Therefore, in the s-VO_x:PSS composite, PSS acts as a dopant for s-VO_x and as a cross-linker, improving the electrical and mechanical properties, respectively, of pristine s-VO_x film. Preparative details for the synthesis of s-VO_x and s-VO_x:PSS are described in the Experimental Section. As shown in Figure S1a (Supporting Information), the prepared s-VO_x:PSS films had excellent transparency with 98% transmittance at 550 nm. Interestingly, the optical bandgap of s-VO_x:PSS film, which was derived from Tauc's formula, was slightly less than that of s-VO_x (Supporting Information, Figure S1b). We speculate that the overlap of band edges and splitting of the doped states induced by PSS in s-VO_x may explain this slight variation. Because PSS can tailor the WF values and act as a cross-linker, eliminating the pin-holes/nanoscopic voids in the TMO films, s-VO_x:PSS is expected to be an efficient HTL in PSCs, as shown in Figure 1b.

2.2. Electronic Structure of s-VO_x and s-VO_x:PSS Films. To investigate the variation in WF of the s-VO_x:PSS films, a Kelvin probe (KP) measurement was performed on the films with various PSS volume ratios.[13] Five samples were prepared on indium tin oxide (ITO) substrates for the KP analysis: ITO/PSS, ITO/s-VO_x, and ITO/s-VO_x:PSS, with 0.4 v/v, 1.0 v/v, and 2.0 v/v PSS. All samples were fabricated from a diluted s-VO_x solution (in IPA with 1:50 v/v) at a low annealing temperature, 80 °C, for 10 min in ambient air.

Figure 2a summarizes the measured WF values for ITO/PSS, ITO/s-VO_x, and ITO/s-VO_x:PSS (with different volume ratios of PSS) electrodes. As the volume of PSS increased, the WF of the HTL/ITO electrodes shifted from 5.0 eV to 5.3 eV. Compared with the previously reported WF values,[23] the s-VO_x shows slightly lower WF values. Because our samples were fabricated in ambient condition, we attribute the difference between the WF values obtained in previous report and in this work to the effect of reduced vanadium oxidation states by air-exposure[24,25](see Supporting Information, Figure S2). Note that the WF values of the s-VO_x:PSS films are higher than those of pristine PSS film (~ 5.1 eV) and s-VO_x (~5.0 eV), indicating that a chemical reaction between s-VO_x and PSS occurred. In addition, it was observed in the capacitance–voltage (C–V) measurement that the carrier density of each film increased with increasing PSS volume (see Supporting Information, Figure S3). These results show that PSS is a promising candidate for efficient doping of s-VO_x.

To compare the energy level alignment between the organic layer and s-VO_x or s-VO_x:PSS, we made a schematic energy level diagram of the PSC structure with these two HTL materials. As shown in Figure 2b, some energy barriers (ΔE_1 = 0.5 eV and ΔE_2 = 0.2 eV) exist between the WF of pristine s-VO_x and the highest occupied molecular orbital (HOMO) of poly[[9-(1-octylnonyl)-9H-carbazole-2,7-diyl]-2,5-thiophenediyl-2,1,3-benzothiadiazole-4,7-diyl-2,5-thiophenediyl] (PCDTBT) or poly[[4,8-bis[(2-ethylhexyl)oxy]benzo[1,2-b:4,5-b′]dithiophene-2,6-diyl][3-fluoro-2-[(2-ethylhexyl)-carbonyl]thieno[3,4-b]thiophenediyl]] (PTB7). However, these barriers are significantly reduced for s-VO_x:PSS. Because the energy barrier at the interface can hinder efficient hole transport from the organic layer to the ITO/s-VO_x electrode, the performance of the device with the s-VO_x:PSS layer should be improved.

The doping mechanism of the s-VO_x:PSS composite was investigated using X-ray photoelectron spectroscopy (XPS) on the pristine s-VO_x and s-VO_x:PSS (1.0 v/v ratio of PSS) films. Figure 2c displays the XPS spectra of $V2p_{3/2}$ and $V2p_{1/2}$ for s-

dx.doi.org/10.1021/am404353y | ACS Appl. Mater. Interfaces 2014, 6, 951–957

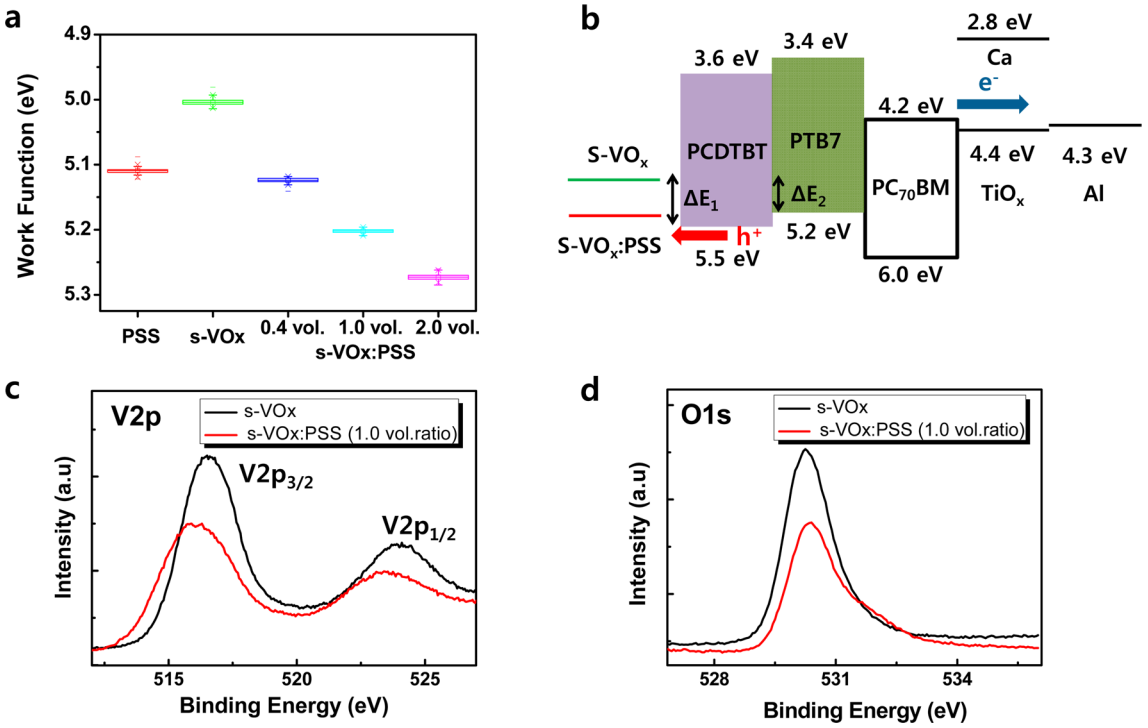

Figure 2. (a) WF values of PSS, s-VO_x, and S-VO_x:PSS (0.4 v/v, 1.0 v/v, and 2.0 v/v ratio) films. (b) Energy level diagram of PSCs and electrical contacts of the HTLs and HOMO of the donor polymers (PCDTBT and PTB7). High resolution XPS spectra of (c) V2p and (d) O1s on s-VO_x and S-VO_x:PSS (1.0 v/v ratio).

Table 1. Photovoltaic Parameters under AM 1.5G Solar Spectrum with a Light Intensity of 100 mW cm^{-2}

	HTLs	V_{oc} [V]	J_{sc} [mA cm^{-2}]	FF	PCE [%]	R_s[a] [Ω cm^2]	R_{sh}[b] [×10^2 Ω cm^2]
PCDTBT: $PC_{71}BM/TiO_x$/Al	PEDOT:PSS	0.86	10.98	0.54	5.14	9.30	4.20
	s-VO_x	0.83	10.86	0.55	5.00	8.40	6.00
	s-VO_x:PSS	0.87	11.16	0.60	5.80	7.20	8.30
PTB7: $PC_{71}BM$/Ca/Al	PEDOT:PSS	0.76	14.14	0.63	6.79	6.60	7.00
	s-VO_x	0.74	13.81	0.64	6.53	6.80	6.40
	s-VO_x:PSS	0.75	14.48	0.65	7.02	6.40	9.50

[a]The R_s of the I-PSCs were calculated using $(dJ/dV)^{-1}$ at $V = V_{oc}$. [b]The R_{sh} of the I-PSCs were calculated using $(dJ/dV)^{-1}$ at $V = 0$.

VO_x and s-VO_x:PSS (1.0 v/v ratio of PSS) films. For the $V2p_{3/2}$ and $V2p_{1/2}$ of the s-VO_x films, the XPS peaks were located at 516.5 eV and 524.04 eV, respectively. However, after adding PSS to VO_x, the peaks shifted to lower binding energies (516.04 eV for $V2p_{3/2}$ and 523.38 eV for $V2p_{1/2}$), corresponding to the reduction in oxidation state of the vanadium atom ($V^{5+} \rightarrow V^{4+}$).[8,24] We attributed the shift in the XPS peaks to the formation of the −V—O—SO_2- complex, which is the result of the chemical reaction between −V═O of the s-VO_x and the sulfonate group ($-SO_3^-$) of the PSS. The shoulder peak (531.5 eV) in the lower binding energy, which corresponds to oxygen bonding to the sulfonate group,[26] supports our hypothesis regarding the doping mechanism in the s-VO_x:PSS composite films. Interestingly, although a partial reduction of the metal oxidation states from V^{5+} to V^{4+} usually decreases the WF values of the metal oxides, the WF of s-VO_x:PSS was larger than that of s-VO_x.[24,25,27] Because there are several reports that the presence of the insulating PSS at the surface strongly attenuate the signal from the bulk materials and increases the WF values,[28,29] we attribute the increased WF of s-VO_x:PSS to the effect of the insulating PSS in the TMO films. The results of XPS data, KP measurement, and C−V analysis clearly show that PSS is a good dopant for s-VO_x.

2.3. Polymer Solar Cells with s-VO_x and s-VO_x:PSS Layers. To explore the effects of s-VO_x:PSS on device performance, we fabricated PSCs with conventional device structures: glass/ITO/HTL/polymer:$PC_{71}BM/TiO_x$(or Ca)/Al, where PEDOT:PSS, s-VO_x, and s-VO_x:PSS were used as HTLs. The devices were tested under air mass 1.5 global (AM 1.5G) condition with an irradiation intensity of 100 mW cm^{-2}. The photovoltaic parameters of these devices are summarized in Table 1. As shown in Figure 3a, the PCDTBT:$PC_{71}BM$ devices with s-VO_x exhibited a PCE of 5% with a short-circuit current density (J_{sc}) of 10.86 mA cm^{-2}, an open-circuit voltage (V_{oc}) of 0.83 V, and a fill factor (FF) of 55%. When HTL was replaced by s-VO_x:PSS, the J_{sc}, V_{oc}, and FF simultaneously increased to 11.16 mA cm^{-2}, 0.87 V, and 60%, respectively, yielding a 5.8% PCE. Because the series resistance (R_s) decreased from 8.40 to 7.20 Ω cm^2 and the shunt resistance (R_{sh}) increased from 600 to 830 Ω cm^2, we speculate that the enhancement in device performance originated from the facilitated charge injection/extraction and reduced charge recombination at the interface of the HTL and the active layer by reducing the energy barrier, ΔE_1, as shown in Figure 2b. To verify the enhancement of the devices, we measured the total absorption (A) of devices from reflectance (R) spectra,

dx.doi.org/10.1021/am404353y | ACS Appl. Mater. Interfaces 2014, 6, 951−957

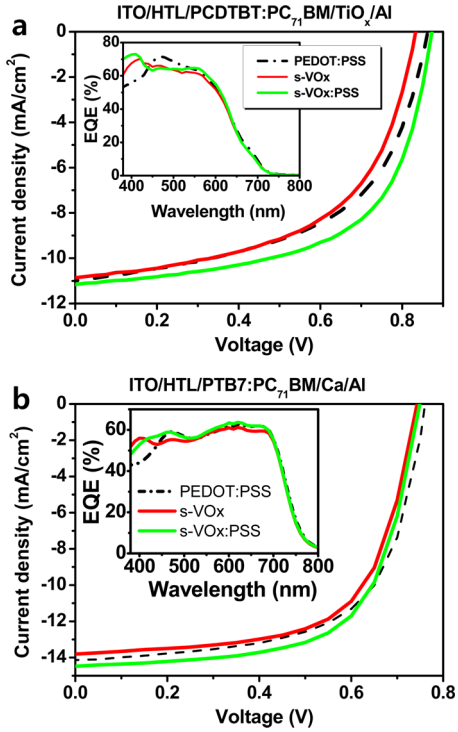

Figure 3. $J-V$ characteristics of (a) ITO/HTL/PCDTBT:$PC_{71}BM$/TiO_x/Al and (b) ITO/HTL/PTB7:$PC_{71}BM$/Ca/Al, where PEDOT:PSS, s-VO_x, and s-VO_x:PSS (1.0 v/v ratio) were used as HTLs. EQE spectra of the devices are also shown in the insets.

using $A = 1 - R$, and calculated the internal quantum efficiency (IQE) values of the devices from the equation of IQE = EQE/A in Figure S3a,b (Supporting Information), respectively. As shown in Figure S3 (Supporting Information), although the A spectra of devices with s-VO_x and s-VO_x:PSS are almost similar in the visible range, the device with s-VO_x:PSS shows the higher IQE than that of s-VO_x. Because the IQE is defined as the ratio of the number of charge carriers collected at the electrodes to the number of photons absorbed by the devices, the higher IQE of the device with s-VO_x:PSS directly indicates that more charge carriers can be extracted by reducing the charge recombination.[30]

A similar result was observed in the PSCs with PTB7 polymer. As shown in Figure 3b, the device with s-VO_x:PSS exhibited an improved PCE of ~7% with a J_{sc} of 14.48 mA cm^{-2}, V_{oc} of 0.75 V, and FF of 65% compared to those of s-VO_x (a PCE of 6.5% with J_{sc} of 13.81 mA cm^{-2}, V_{oc} of 0.74 V, and FF of 64%). In the case of the PTB7:$PC_{71}BM$ PSCs, the J_{sc} was the main factor that enhanced the PCE of the PSCs incorporating s-VO_x:PSS. Because the s-VO_x and s-VO_x:PSS films have similar transparency and the both devices were fabricated using the same processing conditions (especially spin coating speed) with a same BHJ solution, they have similar efficiencies of generation and exciton diffusion of charge carriers. Therefore, we attributed the enhancement of J_{sc} to the increased built-in potential and internal electric field caused by the increased WF of s-VO_x:PSS, which facilitated more efficient sweeping of photo-generated charge carriers.[16]

2.4. Dark Diode Characterization of Devices. To clarify the effect of the s-VO_x:PSS film on device performance, we measured the dark $J-V$ curve of the PSCs incorporating s-VO_x and s-VO_x:PSS. Using the equivalent circuit equation of solar cells, we analyzed the dark $J-V$ curve of PSCs and evaluated the reverse saturation current density (J_0), the diode ideality factor (n), the series resistance (R_s), and the shunt resistance (R_{sh}).[31] The diode parameters of these devices are summarized in Table 2. In the PCDTBT: $PC_{71}BM$ devices, the J_0 and R_{sh} values of PSCs with s-VO_x:PSS were remarkably 50 times (from 1.49×10^{-4} to 3.15×10^{-6} A cm^2) less and 5 times more (from 2.90×10^2 Ω to 1.18×10^3 Ω cm^2) than those of s-VO_x, respectively (Figure 4a). These tendencies were also observed in the PTB7:$PC_{71}BM$ devices, as shown in Figure 4b. Because the J_0 is determined by the number of minority carriers (electrons) in the device, which are able to overcome the energy barrier at the interface between the WF of anode and the LUMO of donor and acceptor molecules under the reverse bias, the reduced J_0 values indicate that the s-VO_x:PSS layer effectively blocked electrons in the devices.[32,33] In addition, the higher R_{sh} implies that the leakage current and charge recombination were effectively suppressed by the s-VO_x:PSS.[34] We can therefore conclude that the s-VO_x:PSS film serves as an effective electron blocking layer that significantly reduces leakage currents in the device and enhances the performance of the PSCs.

2.5. Surface Morphologies of s-VO_x and s-VO_x:PSS Films. The surface morphologies of the s-VO_x and s-VO_x:PSS films were investigated by atomic force microscopy (AFM) measurement. As shown in Figure 5a, the s-VO_x film had an extremely smooth surface morphology with a root-mean-square (RMS) roughness of ~0.6 nm.[17] However, there were many pin-holes/nanoscopic voids throughout the film, which originate from solvent evaporation during film formation.[35] Because the optimum thickness of the s-VO_x film is 10 nm, the pin-holes may decrease the device performance. In the s-VO_x:PSS film, a rougher surface morphology was observed with an RMS value of ~3.2 nm (Figure 5c). Furthermore, no pin-holes/nanoscopic voids were observed in the s-VO_x:PSS film. Because the PSS with a high molecular weight (M_w ~ 75 000) acted as a polymeric cross-linker to form polymer−TMO complex networks, a pin-hole-free film was obtained by

Table 2. Diode Characteristics Obtained from the Dark $J-V$ Characteristic Curves

	HTLs	saturation current density [A cm^{-2}]	diode ideality factor	series resistance[a] [Ω cm^2]	shunt resistance[b] [$\times 10^2$ Ω cm^2]
PCDTBT: $PC_{71}BM$/TiO_x/Al	PEDOT:PSS	7.64×10^{-5}	3.17	4.30	6.20
	s-VO_x	1.49×10^{-4}	3.20	3.10	2.90
	s-VO_x:PSS	3.15×10^{-6}	2.44	2.80	11.8
PTB7: $PC_{71}BM$/Ca/Al	PEDOT:PSS	2.89×10^{-7}	1.82	5.60	4.40
	s-VO_x	2.02×10^{-7}	1.77	5.80	57.3
	s-VO_x:PSS	5.65×10^{-9}	1.46	5.40	91.7

[a]The R_s of the I-PSCs were calculated using $(dJ/dV)^{-1}$ at $V = V_{oc}$. [b]The R_{sh} of the I-PSCs were calculated using $(dJ/dV)^{-1}$ at $V = 0$.

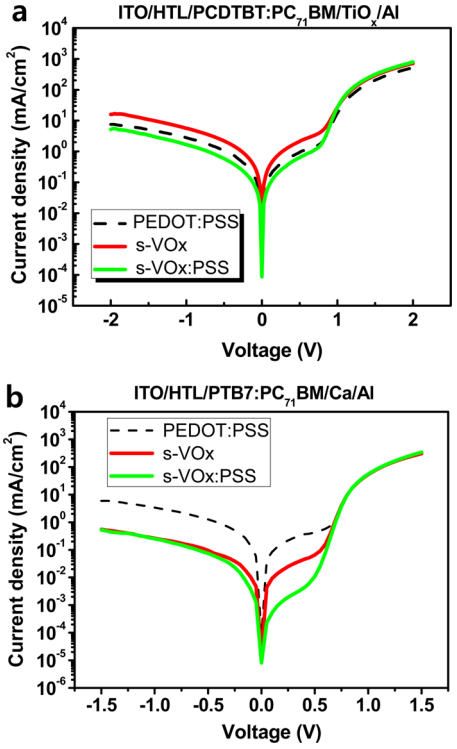

Figure 4. Dark $J-V$ characteristics of (a) ITO/HTL/PCDTBT:$PC_{71}BM$/TiO_x/Al and (b) ITO/HTL/PTB7:$PC_{71}BM$/Ca/Al, where PEDOT:PSS, s-VO_x, and s-VO_x:PSS (1.0 v/v ratio) were used as HTLs.

introducing PSS into s-VO_x. Considering that the thickness of the s-VO_x:PSS layer is ∼20 nm, surface morphology with an RMS value of ∼3.2 nm is not enough to yield a device failure, which is verified from good device performances using the s-VO_x:PSS layer. Therefore, the excellent dark diode characteristics of the device with s-VO_x:PSS can be attributed to the compact surface morphology of the s-VO_x:PSS films. Thus, the film effectively prevented local electrical shorts and/or current leakage at the interface between the HTL and the active layer.

2.6. Stability Measurement of Polymer Solar Cells. The long-term device stability is a very important issue for the commercialization of the PSCs. To verify the stability of s-VOx:PSS, we have compared the stability of PSCs with the device of ITO/HTL/PCDTBT:$PC_{71}BM$/TiO_x/Al, where the HTL layers are PEDOT:PSS, s-VO_x, and s-VO_x:PSS (1.0 v/v ratio.), respectively. Figure 6 shows the device stability of the PSCs as a function of storage time under ambient condition. As shown in Figure 6a, the PCE of the device with PEDOT:PSS continuously decreases with storage time and shows about 50% degradation after 8 days. However, in the case of the s-VO_x and s-VO_x:PSS devices, the PCE still maintains about 80% of their initial values after 8 days in ambient condition. The degradation behaviors of the devices can be further investigated by plotting the J_{sc}, V_{oc}, and FF with storage time. In Figure 6b,c, the J_{sc} and V_{oc} values of devices with PEDOT:PSS, s-VO_x, and s-VO_x:PSS show similar stabilities with storage time. In contrast, the decay of the PEDOT:PSS device is mainly found in a drop of FF as shown in Figure 6d, which originates from structural and electrical vulnerability of PEDOT:PSS in atmospheric humidity.[20,36] Therefore, we attribute the enhanced stability of the devices with s-VO_x and s-VO_x:PSS to the durability of the TMO films in ambient condition. Consequently, the stability of PSCs is significantly improved by replacing the PEDOT:PSS with the newly developed s-VO_x:PSS.

3. CONCLUSION

In conclusion, we developed an effective HTL material based on a composite of solution-processed VO_x and the polymeric acid of PSS to make efficient PSCs. By introducing s-VO_x:PSS composite layers as HTLs, BHJ PSCs showed higher PCE values than PSCs with s-VO_x. The doping s-VO_x with PSS significantly reduced the energy barriers between the active layer and HTLs, thereby facilitating hole transport across the interface. In addition, the pin-hole-free/nanoscopic void-free compact morphology of the s-VO_x:PSS films fabricated by the PSS polymeric template considerably reduced leakage currents in the devices. Furthermore, the PSCs with the s-VO_x:PSS showed promising long-term stability in ambient condition without any encapsulation. Because our approach of combining TMO and polymeric acid shows dramatically better performance than pristine TMO, we expect that it can provide useful guidelines for the synthesis and application of TMOs for organic electronics in the future.

4. EXPERIMENTAL SECTION

4.1. Synthesis of PSS Doped s-VO_x. Soluble vanadium oxide was synthesized by mixing VTIP ($(C_3H_7O)_3VO$, Sigma-Aldrich, 40 μL) precursor and 2 mL of isopropyl alcohol (IPA), which was used as a solvent to make a 1:50 diluted s-VO_x solution. The synthesized s-VO_x solution was very transparent with a slightly yellow color and easily forms uniform films using the spin coating method. For the s-VO_x:PSS solution, PSS ($(C_8H_8O_3S)_n$, Sigma-Aldrich, 18 wt % in H_2O) was added to the 1:50 diluted s-VO_x solution at multiple volume ratios (0.4 v/v, 1.0 v/v, 2.0 v/v) with the VTIP precursor. In contrast to the s-VO_x, the s-VO_x:PSS solution had a strong yellow color. To apply the solution to the devices, the s-VO_x and s-VO_x:PSS (1:50 dilution) products were diluted 1:300 in IPA and spin-cast onto the ITO/glass substrate. The optimized thicknesses of the s-VO_x and s-VO_x:PSS layers were ∼10 and ∼20 nm, respectively. The film thicknesses were measured with SURFCORDER thickness profilometer (Surfcorder ET-3000, Kosaka Laboratory Ltd.).

4.2. Fabrication of PSCs. The patterned ITO/glass substrate (15 Ω/sq) was cleaned with detergent, ultrasonicated in acetone and isopropyl alcohol, and subsequently dried overnight in an oven. After ultraviolet−ozone treating the ITO substrate for 15 min, a 25 nm thick PEDOT:PSS (AI 4083) was spin-cast onto the ITO substrate and dried for 10 min at 150 °C in air. To deposit the photoactive layers, solutions of PCDTBT:$PC_{71}BM$ (1:4) in a dichlorobenzene solvent with a concentration of 7 mg/mL or PTB7:$PC_{71}BM$ (1:1.5) in a chlorobenzene solvent with a concentration of 10 mg/mL were spin-cast onto the PEDOT:PSS/ITO substrate. To fabricate the electron-selective layer of the PSCs, TiO_x precursor solution diluted 1:200 in methanol was spin-cast in air onto the PCDTBT:$PC_{71}BM$ active layer and dried at 80 °C for 5 min in air. Finally, the samples were pumped down to a vacuum (1×10^{-7} Torr; 1 Torr ≈ 133 Pa), and an approximately 100 nm thick Al electrode (area: 14.5 mm^2) was deposited on top of the devices. For the PTB7:$PC_{71}BM$ devices, deposition of the TiO_x layer was not performed; a 20 nm thick Ca electrode and a 100 nm thick Al electrode were sequentially deposited on the photoactive layer in vacuum instead. The $J-V$ characteristics were measured using a Keithley 237 source measure unit in an N_2 atmosphere. Solar cell parameters were obtained by an AM 1.5 G solar simulator with an irradiation intensity of 100 mW·cm^{-2}.

4.3. Characterization of s-VO_x and s-VO_x:PSS Films. For the UV−Vis absorption spectra measurement (PerkinElmer, Lambda 750), pristine s-VO_x and s-VO_x:PSS films were deposited on fused silica substrates. Total absorption spectra of PCDTBT:$PC_{71}BM$ PSCs were measured using the UV−Vis absorption spectra measurement (PerkinElmer, Lambda 750, USA) system in reflection mode. The XPS

dx.doi.org/10.1021/am404353y | ACS Appl. Mater. Interfaces 2014, 6, 951−957

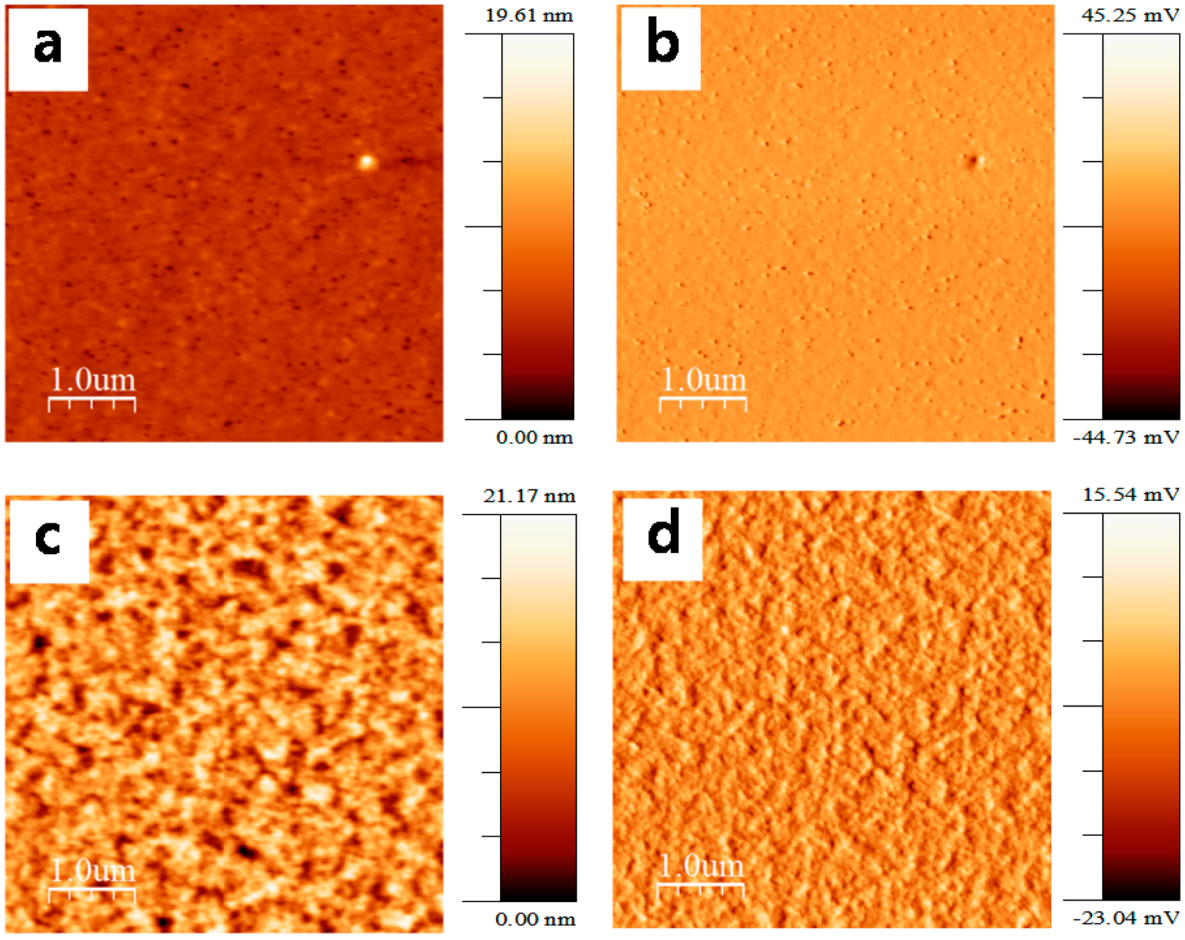

Figure 5. Topography AFM images of (a) s-VO_x and (c) s-VO_x:PSS films on ITO substrates. Phase AFM images of (b) s-VO_x and (d) s-VO_x:PSS films are also shown.

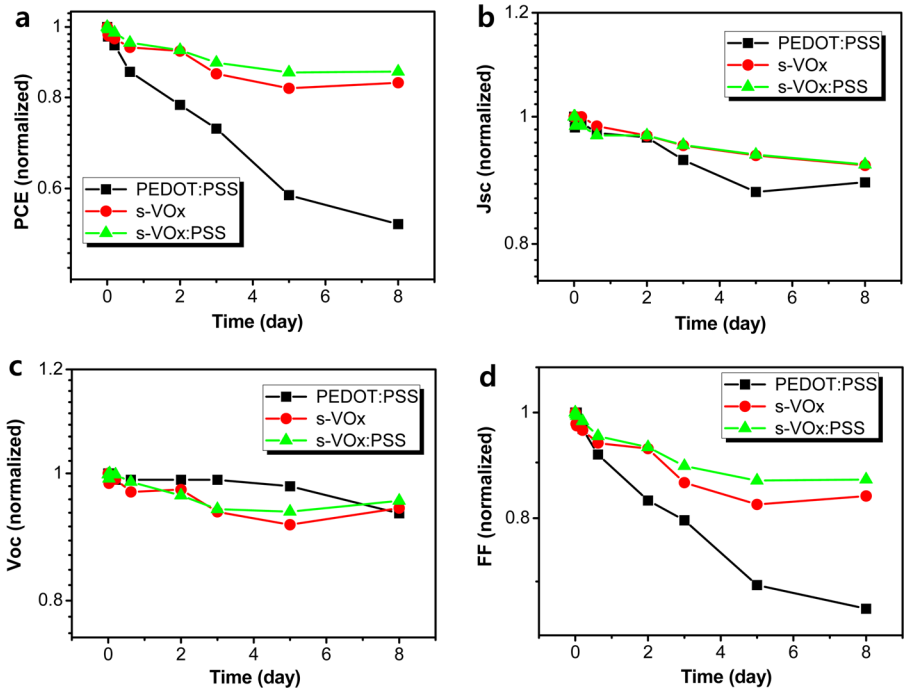

Figure 6. Normalized (a) PCE, (b) J_{sc}, (c) V_{oc}, and (d) FF values for PSCs with the device of ITO/HTL/PCDTBT:$PC_{71}BM$/TiO_x/Al, where the HTL layers are PEDOT:PSS, s-VO_x, and s-VO_x:PSS (1.0 v/v ratio.), respectively, as a function of storage time in air under ambient conditions.

dx.doi.org/10.1021/am404353y | ACS Appl. Mater. Interfaces 2014, 6, 951−957

measurement was performed using a MultiLab 2000 (Thermo electron corporation) with an Al Kα source in an approximately 7.5×10^{-10} Torr vacuum in the Center for Research Facilities of Chonnman National University, Republic of Korea. All spectra were calibrated with the C 1s peak at 285 eV. The UPS measurement was performed using UPS measurement in Daejeon Center of Korea Basic Science Institute (KBSI). The measurements were performed by using an equipment of AXIS-NOVA (Kratos Analytical Ltd) with a He I (21.2 eV) excitation source in an ultrahigh vacuum of 1.0×10^{-10} Torr. The WF values of the s-VO_x and s-VO_x:PSS films were measured using a Kelvin probe (KP 6500 Digital Kelvin probe, McAllister Technical Services. Co. Ltd) in atmospheric conditions.

■ ASSOCIATED CONTENT

Supporting Information

Transmission spectra (Figure S1), work function values of samples processed in N_2 condition (Figure S2), capacitance-voltage measurement (Figure S3), charge carrier density (Table S1) of s-VO_x and s-VO_x:PSS films are provided here. Total absorption and internal quantum efficiency (Figure S4) of devices incorporating s-VO_x and s-VO_x:PSS are also provided. This material is available free of charge via the Internet at http://pubs.acs.org.

■ AUTHOR INFORMATION

Corresponding Authors

*Heejoo Kim. E-mail: heejook@gist.ac.kr.
*Kwanghee Lee. E-mail: klee@gist.ac.kr.

Notes

The authors declare no competing financial interest.

■ ACKNOWLEDGMENTS

This work was supported by the Core Technology Development Program for Next-Generation Solar Cells of the Research Institute for Solar and Sustainable Energies (RISE) at GIST and the National Research Foundation (NRF) of Korea (No. 20110030962). The authors also acknowledge the support provided by the National Research Foundation of Korea (NRF) grant, funded by the Korean government (MSIP) (No. 2008-0062606, CELA-NCRC). This work was also supported by a National Research Foundation of Korea (NRF) grant, funded by the Korean government (MSIP) (No. 2008-0093869). The author also thanks B. Son for UPS measurement in Daejeon Center of Korea Basic Science Institute (KBSI).

■ REFERENCES

(1) Kim, J. Y.; Lee, K.; Coates, N. E.; Moses, D.; Nguyen, T.-Q.; Dante, M.; Heeger, A. J. *Science* **2007**, *317*, 222−225.
(2) Small, C. E.; Chen, S.; Subbiah, J.; Amb, C. M.; Tsang, S.-W.; Lai, T.-H.; Reynolds, J. R.; So, F. *Nat. Photon.* **2012**, *6*, 115−120.
(3) Chen, L.-M.; Xu, Z.; Hong, Z.; Yang, Y. *J. Mater. Chem.* **2010**, *20*, 2575−2598.
(4) Steim, R.; Kogler, F. R.; Brabec, C. J. *J. Mater. Chem.* **2010**, *20*, 2499−2512.
(5) Kim, J. Y.; Kim, S. H.; Lee, H. H.; Lee, K.; Ma, W.; Gong, X.; Heeger, A. J. *Adv. Mater.* **2006**, *18*, 572−576.
(6) Sun, Y.; Seo, J. H.; Takacs, C. J.; Seifter, J.; Heeger, A. J. *Adv. Mater.* **2011**, *23*, 1679−1683.
(7) Manders, J. R.; Tsang, S.-W.; Hartel, M. J.; Lai, T.-H.; Chen, S.; Amb, C. M.; Reynolds, J. R.; So, F. *Adv. Funct. Mater.* **2013**, *23*, 2993−3001.
(8) Xie, F.; Choy, W. C. H.; Wang, C.; Li, X.; Zhang, S.; Hou, J. *Adv. Mater.* **2013**, *25*, 2051−2055.
(9) Sun, Y.; Takacs, C. J.; Cowan, S. R.; Seo, J. H.; Gong, X.; Roy, A.; Heeger, A. J. *Adv. Mater.* **2011**, *23*, 2226−2230.
(10) Ma, H.; Yip, H.-L.; Huang, F.; Jen, A. K. Y. *Adv. Funct. Mater.* **2010**, *20*, 1371−1388.
(11) Choi, H.; Cho, H.; Song, S.; Suh, H.; Park, S.; Kim, J. Y. *Phys. Chem. Chem. Phys.* **2010**, *12*, 15309−15314.
(12) Kofstad, P. *Oxid. Met.* **1995**, *44*, 3−27.
(13) Kim, J.; Kim, G.; Choi, Y.; Lee, J.; Park, S. H.; Lee, K. *J. Appl. Phys.* **2012**, *111*, 114511−9.
(14) Pomoni, K.; Vomvas, A.; Trapalis, C. *Thin Solid Films* **2005**, *479*, 160−165.
(15) Choi, H.; Park, J. S.; Jeong, E.; Kim, G.-H.; Lee, B. R.; Kim, S. O.; Song, M. H.; Woo, H. Y.; Kim, J. Y. *Adv. Mater.* **2011**, *23*, 2759−2763.
(16) Kyaw, A. K. K.; Wang, D. H.; Gupta, V.; Zhang, J.; Chand, S.; Bazan, G. C.; Heeger, A. J. *Adv. Mater.* **2013**, *25*, 2397−2402.
(17) Stubhan, T.; Salinas, M.; Ebel, A.; Krebs, F. C.; Hirsch, A.; Halik, M.; Brabec, C. J. *Adv. Energy Mater.* **2012**, *2*, 532−535.
(18) Liao, S.-H.; Jhuo, H.-J.; Cheng, Y.-S.; Chen, S.-A. *Adv. Mater.* **2013**, *25*, 4766−4771.
(19) Park, S. Y.; Kim, B. J.; Kim, K.; Kang, M. S.; Lim, K.-H.; Lee, T. I.; Myoung, J. M.; Baik, H. K.; Cho, J. H.; Kim, Y. S. *Adv. Mater.* **2012**, *24*, 834−838.
(20) Zilberberg, K.; Trost, S.; Schmidt, H.; Riedl, T. *Adv. Energy Mater.* **2011**, *1*, 377−381.
(21) Lang, U.; Müller, E.; Naujoks, N.; Dual, J. *Adv. Funct. Mater.* **2009**, *19*, 1215−1220.
(22) Elschner, A.; Kirchmeyer, S.; Lovenich, W.; Merker, U.; Reuter, K. *PEDOT: Principles and Applications of an Intrinsically Conductive Polymer*; Taylor & Francis: New York, 2010; Vol. *1*, p 117.
(23) Hancox, I.; Rochford, L. A.; Clare, D.; Walker, M.; Mudd, J. J.; Sullivan, P.; Schumann, S.; McConville, C. F.; Jones, T. S. *J. Phys. Chem. C* **2012**, *117*, 49−57.
(24) Zilberberg, K.; Trost, S.; Meyer, J.; Kahn, A.; Behrendt, A.; Lützenkirchen-Hecht, D.; Frahm, R.; Riedl, T. *Adv. Funct. Mater.* **2011**, *21*, 4776−4783.
(25) Meyer, J.; Hamwi, S.; Kröger, M.; Kowalsky, W.; Riedl, T.; Kahn, A. *Adv. Mater.* **2012**, *24*, 5408−5427.
(26) Yan, H.; Okuzaki, H. *Synth. Met.* **2009**, *159*, 2225−2228.
(27) Zilberberg, K.; Meyer, J.; Riedl, T. *J. Mater. Chem. C* **2013**, *1*, 4796−4815.
(28) Lee, T.-W.; Chung, Y. *Adv. Funct. Mater.* **2008**, *18*, 2246−2252.
(29) Yeo, J.-S.; Yun, J.-M.; Kim, D.-Y.; Park, S.; Kim, S.-S.; Yoon, M.-H.; Kim, T.-W.; Na, S.-I. *ACS Appl. Mater. Interfaces* **2012**, *4*, 2551−2560.
(30) Park, S. H.; Roy, A.; Beaupre, S.; Cho, S.; Coates, N.; Moon, J. S.; Moses, D.; Leclerc, M.; Lee, K.; Heeger, A. J. *Nat. Photonics* **2009**, *3*, 297−302.
(31) Lee, J. H.; Cho, S.; Roy, A.; Jung, H.-T.; Heeger, A. J. *Appl. Phys. Lett.* **2010**, *96*, 163303−3.
(32) Waldauf, C.; Scharber, M. C.; Schilinsky, P.; Hauch, J. A.; Brabec, C. J. *J. Appl. Phys.* **2006**, *99*, 104503−6.
(33) Dorf, R. C. *The Electrical Engineering Handbook*; CRC Press: New York, 1997; Vol *1*, p 501.
(34) Steim, R.; Choulis, S. A.; Schilinsky, P.; Brabec, C. J. *Appl. Phys. Lett.* **2008**, *92*, 093303−3.
(35) Orignac, X.; Vasconcelos, H. C.; Du, X. M.; Almeida, R. M. *J. Sol−Gel Sci. Technol.* **1997**, *8*, 243−248.
(36) de Jong, M. P.; van IJzendoorn, L. J.; de Voigt, M. J. A. *Appl. Phys. Lett.* **2000**, *77*, 2255−2257.